



Research Article

Performance Enhancement of Parabolic Dish Collector Receiver Using Phase Change Material: A CFD Simulation

Reza Roohi ^{a*}, Masoud Akbari ^a

^a Department of Mechanical Engineering, School of Engineering, Fasa University, P. O. Box: 74617-81189, Fasa, Iran.

PAPER INFO

Paper history:

Received: 02 July 2022

Revised: 08 December 2022

Accepted: 18 December 2022

Keywords:

Parabolic Dish Collector,
Phase Change Material,
Solar Energy,
CFD Simulation

ABSTRACT

The design of novel and effective receivers is one of the most challenging aspects of solar energy harvesters, especially for Parabolic Dish Collectors (PDCs). The variation of solar flux due to the solar time and sky clearance index can affect the output thermal energy of the collector. One of the major approaches to producing a uniform performance for the PDCs is the utilization of Phase Change Materials (PCMs). The PCMs can absorb the solar flux at its peak instances. Subsequently, due to the thermal buffering effect, excess energy is released in cases with lower solar flux. In the present study, a novel design of receiver with multiple layers of thin PCM inserted between the passages of the working fluid is numerically simulated. The simulations are designed to determine the effect of operational parameters on the performance of the examined novel receiver. According to the results, by increasing the Heat Transfer Fluid (HTF) flow rate from 60 to 90 kg/h, the system efficiency is increased from 53.8 to 66.4 %.

<https://doi.org/10.30501/jree.2023.349281.1393>

1. INTRODUCTION

The use of solar energy as a globally available, clean energy source has been on the rise lately ([Kousik and Natarajan, 2022](#); [Panchal and Patel, 2018](#); [Kabeel et al., 2022](#); [Sonawane et al., 2022](#); [Sonawane et al., 2022](#); [Panchal et al., 2021](#); [Palanikumar et al., 2021](#); [Saleh et al., 2022](#); [Felemban et al., 2022](#)). Among several approaches to utilizing renewable solar energy, Parabolic Dish Collectors (PDCs) have received less attention or optimization than other more common types, namely flat plate collectors (FPCs) ([Natarajan et al., 2019](#)), parabolic through collectors (PTCs) ([Reddy and Kumar, 2009](#)), and energy storage systems ([Suraparaju et al., 2021](#)). Despite the fact that the receiver of PDCs has been scrutinized by a number of optimization researches due to the high amount of reflected radiation flux, major challenges still remain to determine the optimum type and configuration setup in various operating conditions ([Taumoefolau et al., 2021](#)).

The usage of Phase Change Materials (PCMs) ([Suraparaju and Natarajan, 2021](#)) is one of the methods employed to improve the efficiency of solar thermal energy systems ([Sampathkumar and Natarajan, 2022](#)). PCMs undergo a melting and solidification cycle by heating and cooling around a specified thermal range with a considerable amount of enthalpy change, which can be used to improve the system thermal behavior ([Suraparaju and Natarajan, 2022](#)).

Several researchers examined the idea of using PCM in the configuration of PDCs ([Thakur et al., 2022](#)). Senthil and

Cheralathan ([Senthil and Cheralathan, 2019](#)) investigated the ability of storage improvement of a PDC using the PCM experimentally. They used the PCM as thin layers between the passage routes of the Heat Transferring Fluid (HTF). The performance of the system was tested at different flow rates of the HTF and it was concluded that a more uniform thermal output could be obtained even in discontinuities in the solar flux. Besides, they found that the PCM receiver could be treated as a thermal battery to provide sufficient energy, even after the sunset.

The thermal conductivity of the PCM in the receiver can be enhanced using metallic meshes ([Khalil Anwar et al., 2016](#)). Still, in some cases, the absorbed sensible heat after melting of the PCM creates hot spots in the domain and prevents the formation of a uniform thermal field within the receiver ([Yilbasa and Khalil Anwar, 2016](#)).

The maximum exergy destruction ([Mazzucco et al., 2018](#)), the transient behavior of temperature field ([Avargani et al., 2016](#)), and the local temperature distribution in the receiver ([Ren et al., 2018](#)) are some of the major topics studied by the researchers regarding the performance of PDC.

The improvement of the thermal performance of the PCM receiver using fine metallic particles was reported in ([Saleem et al., 2018](#)). The enhanced thermal conductivity using the mentioned modification produces a more uniform thermal field and better exergetic efficiency, as well.

*Corresponding Author's Email: Re.roohi@fasau.ac.ir (R. Roohi)

URL: https://www.jree.ir/article_164087.html



Peiro et al., (Peiro et al., 2018) investigated the effect of PCMs in multiple and single scenarios. D-mannitol and hydroquinone were implemented as PCMs for which the phase change occurred between 420 and 470 K. According to the obtained results, the use of multiple PCMs can improve the system thermal performance by about 20% and produce a more uniform thermal field than the case with individual PCM.

The examination of the best choice of eutectic solder for domestic energy storage among three choices of polyethylene, erythritol, and adipic acid was conducted by Mawire et al. (Mawire, et al., 2019). The PCM configuration was spherical and the operating temperature was around 100 °C. According to the results, the best material for the studied application was Erythritol.

A novel design of solar cooker using parabolic concentrator was proposed by Shanthi Rekha and Sukchai (Santhi Rekha and Sukchai, 2018). Concentric hollow cylinder was used as an inner layer, and the vertical PCM rods were implemented as the outer layer. The utilization of the PCM enhanced the cooker optical efficiency factor up to 100%.

The design and examination of novel receivers were performed by several researchers (Tharun et al., 2022). A modified conical cavity receiver was proposed in (Kopalakrishnaswami and Natarajan, 2022) to minimize the thermal loss from the receiver (Singh and Natarajan, 2021).

In the present study, the performance of a PDC receiver with multiple layers of PCM is numerically simulated to ensure a better understanding of the system performance, which is missing in the current literature. The solar flux distribution on the receiver is determined based on the Discrete Ordinate (DO) radiation model. The energy, flow, and phase change equations with proper boundary conditions were solved to determine the temperature, velocity, and liquid fraction fields. The effect of HTF mass flow rate on the system thermal efficiency is determined. In a moderate period of time (about 20 min), the reduction or absence of solar flux has negligible impact on the output thermal efficiency, which is promising in practical situations.

2. MATHEMATICAL MODELING

2.1. Problem description

The examined receiver structure consists of HTF passages around the confined zones of PCM (erythritol) to exchange heat during melting and solidification phases. The schematics of the simulated configuration from various views are illustrated in Figure 1.

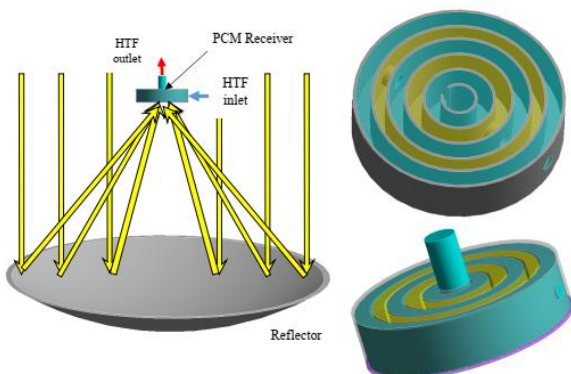


Figure 1. The schematics of the simulated configuration from various views.

As the density of the PCM reduces during melting, 20% of its container remains empty at the room temperature. The thermo-physical properties of erythritol are listed in Table 1.

Table 1. Thermophysical properties of erythritol (Suraparaju and Natarajan, 2021).

Property	Erythritol		Water	
	Value	Unit	Value	Unit
Latent heat	339	kJ/kg		kJ/kg
Melting point	390	K		K
	Solid phase (293 K)	Liquid phase (413 K)	-	-
Thermal conductivity	0.733	0.326	W/m.K	W/m.K
Density	1480	1300	kg/m ³	kg/m ³
Specific heat	1.38	2.76	kJ/kg.K	kJ/kg.K

2.2. Initial and boundary condition

To simulate a realistic case, the initial and boundary conditions should be assigned according to the receiver operational status. The irradiation flux on the glass cover varies according to the solar time and the concentration ratio of the examined solar concentrator.

The peripheral area of the receiver is assumed to be adiabatic to prevent heat loss. The list of operational conditions with their range of variations arise presented in Table 2.

Table 2. Operational condition of PCM receiver.

Parameter	Value	Unit
PCM material	erythritol	
HTF material	Water	
HTF inlet temperature	300	K
HTF mass flow rate	60, 70, 80 and 90	kg/h
Solar irradiation intensity	Variable with time according to Figure. 3	W/m ²
Solar flux distribution on receiver	According to Eq. 7	W/m ²
Geometrical parameters		
Glass thickness	0.5	Mm
HTF inlet diameter	12.5	mm
HTF outlet diameter	25.0	mm
Rib's spacing	25.0	mm
Receiver width	100	mm
Receiver diameter	406	mm

It should be mentioned that to avoid unnecessary complexities during the numerical simulation, the following assumptions are made: The thermo-physical properties are assumed to be constant during the simulation, except density which is obtained based on the Boussinesq assumption (to prevent unnecessary complexities in the CFD simulation process). The system initial temperature is 300 K throughout the domain. The wind velocity which affects the convection heat transfer coefficient on the glass cover as well as the HTF inlet temperature are constant during the simulation. The viscous dissipation as well as the non-Newtonian behavior of the PCM liquid phase are also ignored (according to their less significant

effect than other heat transfer mechanisms such as solar irradiation, convection, and conduction heat transfer mechanisms).

2.3. Governing equations

2.3.1. Fluid domain

To determine the flow and temperature pattern in the fluid zones (including the HTF and PCM), the transient and coupled continuity, momentum, and energy equations should be solved. The coupling between the energy and flow governing equations is due to the presence of natural convection heat transfer.

The continuity equation can be formulated as:

$$\frac{\partial \rho}{\partial t} + \nabla \cdot (\rho \vec{V}) = 0 \quad (1)$$

The momentum equation in Cartesian coordinate system using the Boussinesq approximation can be written as:

$$\rho \left(\frac{\partial \vec{V}}{\partial t} + \vec{V} \cdot \nabla \vec{V} \right) = -\nabla P + \mu \nabla^2 \vec{V} + \rho \vec{g} \beta (T - T_0) + \vec{S} \quad (2)$$

The source term in the momentum equation (\vec{S}) is estimated as follows:

$$\vec{S} = \frac{(1 - \alpha^2)}{(\alpha^2 + \varepsilon)} A_{mz} (\vec{V} - \vec{V}_{pull}) \quad (3)$$

The momentum source term is applied as a velocity damping factor between zero velocity at the solid interface and maximum velocity at the fluid interface. The parameter A_{mz} is a mushy zone coefficient that has a common value between 10^4 and 10^7 . \vec{V}_{pull} is the pull velocity due to the solids extraction and the ε value at the denominator is a negligible number, which prevents division to zero. The liquid fraction (α) is directly related to the phase change temperatures (T_l and T_s) and is defined as:

$$\alpha = \begin{cases} 0 & T < T_s \\ \frac{T - T_s}{T_l - T_s} & T_s \leq T \leq T_l \\ 1 & T > T_l \end{cases} \quad (4)$$

The energy equation is formulated as follows:

$$\frac{\partial (h_t)}{\partial t} + \nabla \cdot (\vec{V} h_t) = \nabla \cdot \left(\frac{k}{\rho c_p} \nabla h_s \right) \quad (5)$$

where the total enthalpy (h_t) is the summation of sensible (h_s) and latent (h_l) enthalpies.

2.3.2. Solid domain

For the solid parts of the domain including the receiver structure and glass cover, the unsteady 3D form of conduction heat transfer is incorporated as:

$$\rho c_p \frac{\partial (T)}{\partial t} = \nabla \cdot (k \nabla T) + \dot{q} \quad (6)$$

where ρ , c_p , k , T , and \dot{q} are density, specific heat capacity, thermal conductivity of the domain, temperature, and volumetric heat generation, respectively. It should be noted that the volumetric heat generation mechanism merely occurs in the glass cover due to the radiation absorption and is calculated based on the Discrete Ordinate (DO) radiation model.

2.4. Numerical considerations

The mentioned set of coupled governing equations is solved numerically using the finite volume discretization method. For the pressure-velocity coupling, a simple algorithm is incorporated as the comparison with other coupling algorithms shows negligible improvement in the results. The discretization of the momentum and energy equations is performed using the first-order upwind equation while the PRESTO method is applied for the pressure corrections. To ensure the convergence of the simulation, the mean relative errors in continuity, momentum, and energy equations are calculated and compared with the convergence criteria of 10^{-4} , 10^{-4} , and 10^{-7} respectively.

The simulation is carried out on a system with computational hardware of Intel® Xeon® Processor E6540 (18M Cache, 2.00 GHz, 16 GB RAM) featuring a Windows 10 operating system (64-bit). Each simulation lasted about 16 hours.

2.4.1. Computational domain

The utilized computational cells are given in Figure 2 from different points of view. To obtain sufficiently accurate results, the concentration and structure of grid cells should be related to the flow regime. To do so, the boundary layer type cells at the solid walls as well as finer cells in melting regions are employed. According to the performed grid study, the suitable number of grid points for the present study is about 463,000 cells.

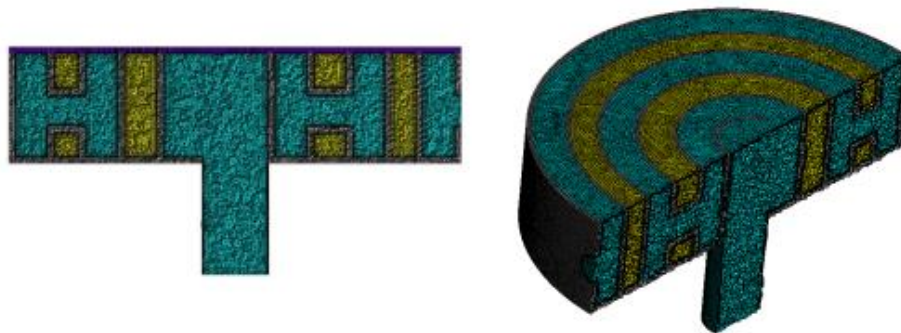


Figure 2. The utilized computational cells.

2.5. Solar Irradiation flux

The solar flux in the receiver is calculated using the SOLTRACE software (Varun et al., 2020) based on the geometrical and optical parameters. The inputs of the software include the sun's information, characteristics of the examined optical elements, dish collector, and receiver geometry as well as the number of emitted rays. In the current examination, the Gaussian model for the sun's shape and a normal direct intensity of 663.4 W/m² is set in the modeling. As the number of emitted rays has direct influence on the accuracy of the obtained results (especially for flux distribution created by concentrating reflectors), a sensitivity analysis on the mentioned parameter is performed. Four different ray numbers namely 104, 105, 106, and 107 are considered and according to the results, it has been proved that the 106 rays are adequate for precise estimation of solar flux .

Based on the systems properties (Tables 3 and 4), the flux distribution of the solar irradiation of the receiver surface and the irradiation ray tracing pattern is given in Figures 3 and 4, respectively.

Table 3. Geometric parameters and optical properties of the parabolic dish.

Parameter	Value
Diameter	4.175 m
Focal length	4.5 m
Reflectivity	92%
Transmissivity	8%

Table 4. SolTrace modeling parameters.

Parameter	Value
The reflectance of the cavity walls	0.15
Number of ray intersections	100 000
The optical errors	10 mrad
The half-angle width	4.65 mrad

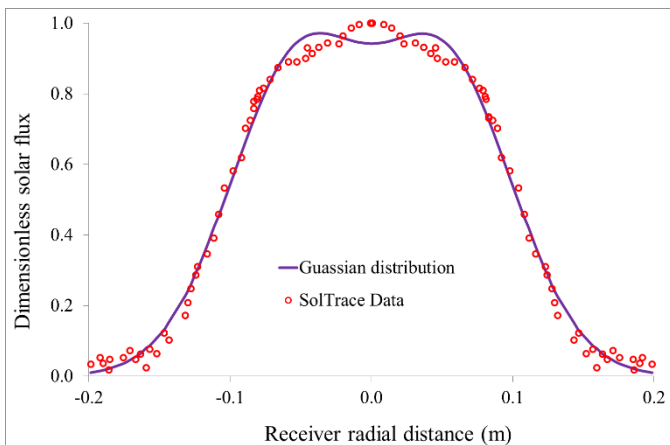


Figure 3. The incident solar flux reflected on the receiver.

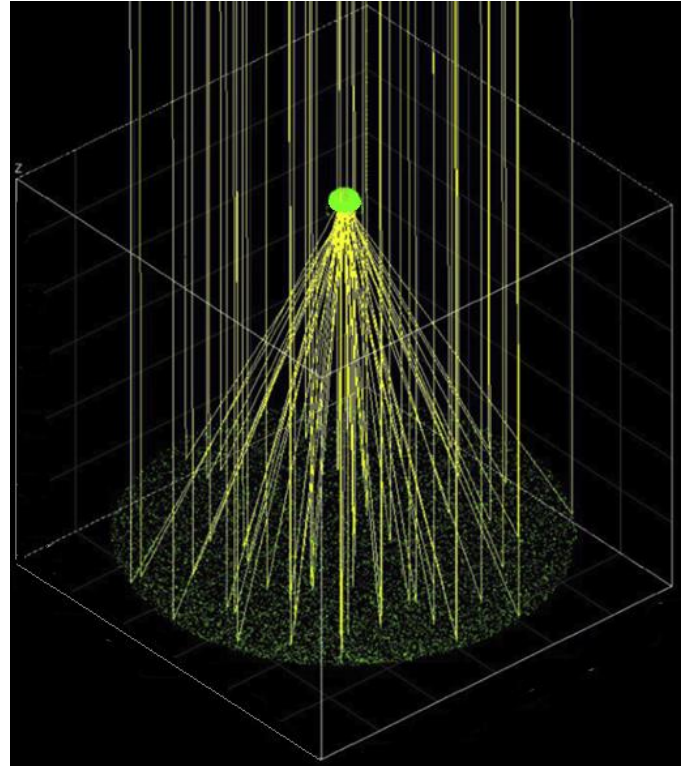


Figure 4. The irradiation ray tracing pattern.

The incident solar flux reflected on the receiver is given in Figure 3. The data is extracted from the SolTrace simulation. The presented data is approximated by a Gaussian distribution to be imported in the CFD simulation. It is obvious that the Gaussian curve resembles the flux distribution with acceptable deviation (*i.e.*, $R^2 = 0.989$). The curve formulation employed in the CFD simulation is:

$$Q = a_1 e^{-\left(\frac{r-b_1}{c_1}\right)^2} + a_2 e^{-\left(\frac{r-b_2}{c_2}\right)^2} \tag{7}$$

Coefficients of Eq. (7):

a_1	b_1	c_1	a_2	b_2	c_3
-6.52e5	-2.93e-5	0.0613	1.23e6	-2.16e-5	0.0870

3. RESULTS AND DISCUSSION

The velocity contours and vectors at a plane passing through the horizontal middle plane are shown in Figure 5 at different inlet mass flow rates. As it is obvious, the velocity at the zones containing solid phase is zero. At the lowest simulated inlet velocity (Figure 5-a), the lack of a uniform flow stream passing through the spiral pathway is observable. This observation is based on the velocity vector patterns in Figure 5-1. However, by increasing the inlet mass flow rate, the velocity vectors and contours reveal a uniform, enhanced flow field that intensifies the system capability to absorb the radiated thermal energy. Moreover, the contraction of the flow and increase in the flow velocity passing through the implemented channels between external and internal zones can be seen in Figure 6.

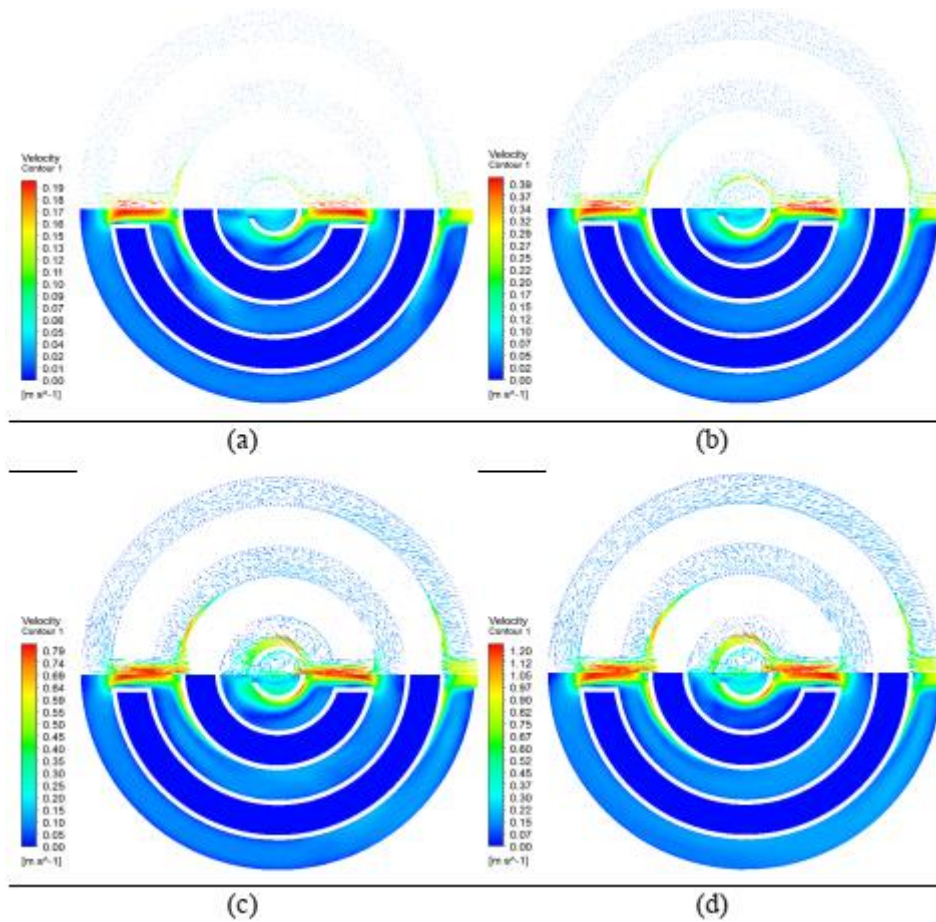


Figure 5. The velocity contours and vectors at a plane passing through the horizontal middle plane: a) 60, b) 70, c) 80, and d) 90 kg/h..

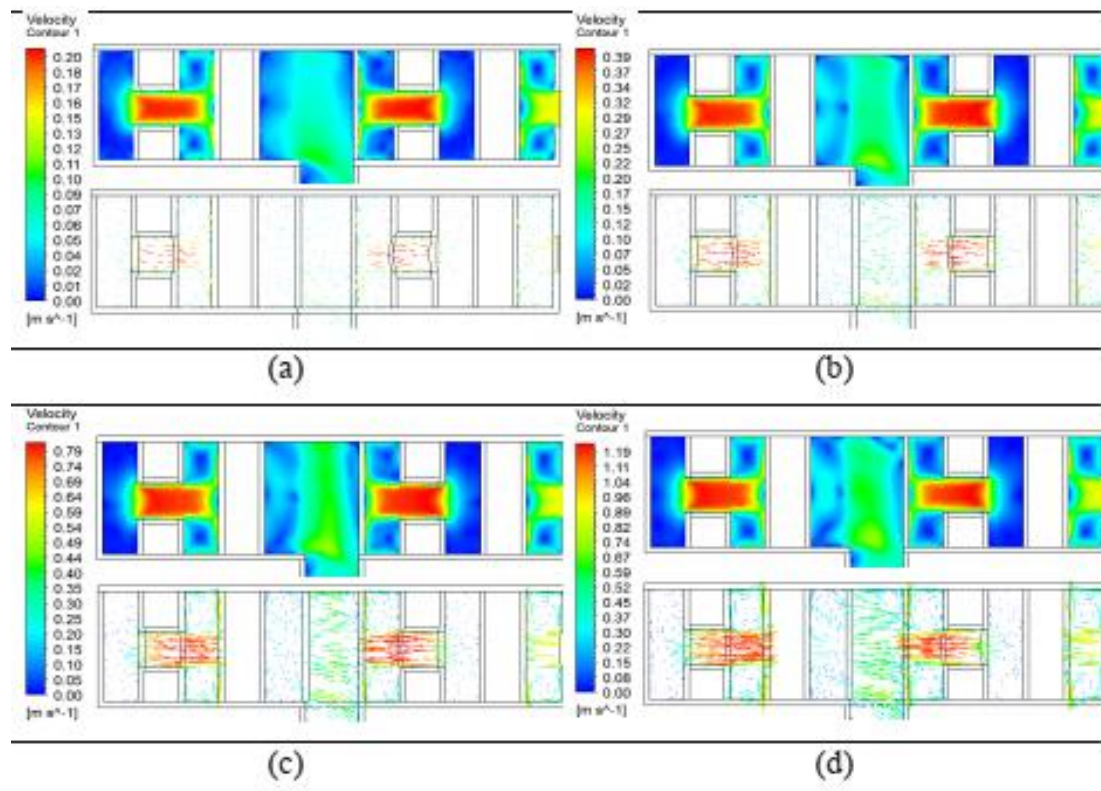


Figure 6. The velocity contours and vectors at a plane passing through the vertical middle plane: a) 60, b) 70, c) 80, and d) 90 kg/h.

The variation of the flow temperature as well as the path lines are illustrated in Figure 7. According to Figure 7, as the fluid enters the absorber from the entrance area on the peripheral side, an initial swirl is spotted due to its collision with the outside solid zone wall. This wall reroutes the flow as a blunt obstacle. Then, the flow stream becomes almost uniform in the second half of the outside channel. The same behavior is repeated after the flow enters the middle channel with a slight difference that the uniform flow cannot be reached due to the short flow passage. Finally, the heated flow enters the central section and exits perpendicular to the outlet section.

According to the obtained results, the temperature increase rate is not the same along the passage of the flow stream. In the outer loop, the temperature increase has an average magnitude of 2.8 °C. However, the middle flow loop increases the temperature to about 8.8 °C and the temperature growth in the central section is 9.5 °C. Despite the fact that the flow path in the outer loop is longer and a higher temperature increase is expected, two major reasons contribute to the enhancement of higher temperature in the internal loops. These reasons are the higher irradiation flux by motion toward the receiver center (based on the nature of reflection pattern from the reflector) and higher thermal absorption in the PCM material for the inner solid channel, as well. This is because the inner channel is placed within two zones of PCM.

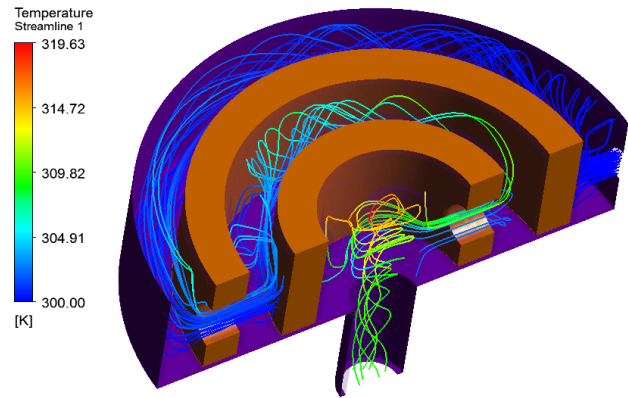


Figure 7. The variation of flow temperature along the path lines.

The liquid fraction as a performance measure of the absorber PCM section is given in Figure 8 at different flow rates. At lower inlet velocities (Figure 8-a), as the residence time of the fluid in the receiver lengthens, the higher amount of thermal energy is absorbed and the fluid temperature is increased, as well. So, in case of lower inlet mass flow rates, the elevated fluid temperature increases the chance of phase change in the PCM section. Besides, it is obvious that even in the outer channel, a thin layer of melted PCM is also created. This phenomenon does not occur at higher inlet mass flow rates, as all of the phase change occurs merely in the inner solid section at higher flow rates (i.e., Figure 8-b to d).

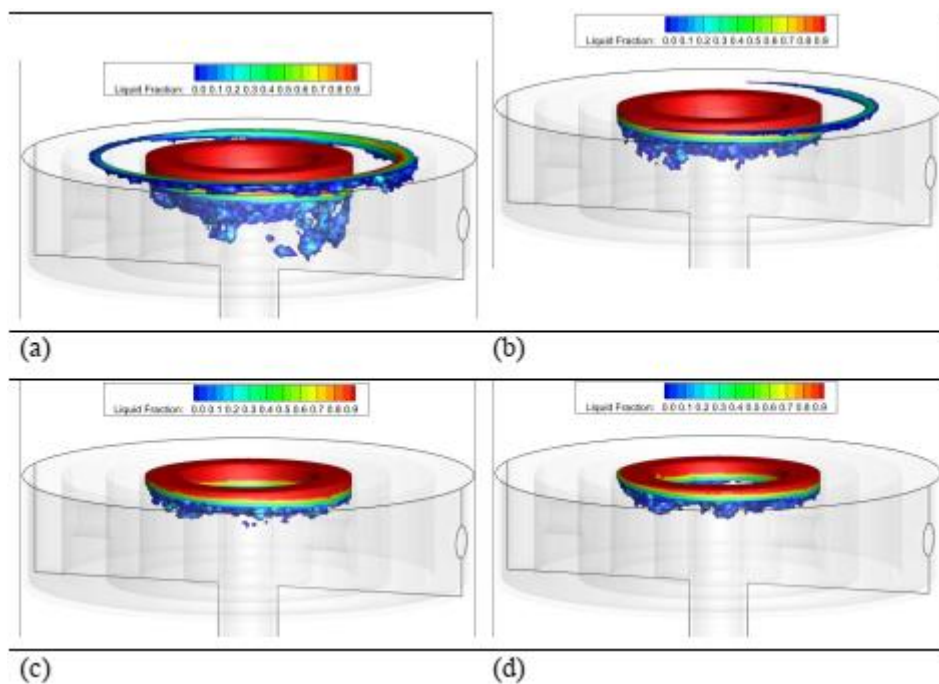


Figure 8. The PCM liquid fraction contours for a) 60, b) 70, c) 80, and d) 90 kg/h.

The depth of the melted zone is also another important parameter that should be noticed. For all of the examined cases, the top surface of the inner section is completely melted due to the direct exposure to the solar flux and temperature increase beyond the melting point. However, the depth at which the phase change occurs has a direct relation to the flow velocity. With the exception of inlet mass flow rate of 60 kg/h, the phase change is limited in other cases to the region in the vicinity of the upper surface. Besides, in case of minimum inlet velocity at

which the two-phase region penetrates into the system, the circumferential distribution of the liquid mass fraction is not uniform due to the variations of geometrical and fluid characteristics in the circumferential direction.

The effect of HTF flow rate on the thermal efficiency of the PDC enhanced with the PCM layers is given in Figure 9. According to the results, by increasing the HTF flow rate from 60 to 90 kg/h, the system efficiency is increased from 53.8 to 66.4 %. As the mass flow rate of HTF is increased by 10 kg/h,

the rate of efficiency enhancement is higher at low mass flow rates. In other words, the same flow rate increase leads to 10% and 6% relative efficiency increase at mass flow rates of 60 and 90 kg/h, respectively .

Moreover, it is observed that the presence of multilayer PCM fields can preserve the uniform pattern of thermal energy absorption even in the intermittent or full cloudy sky. In a moderate period of time (about 20 min), the reduction or absence of solar flux has negligible impact on the output thermal efficiency, which is promising in practical situations.

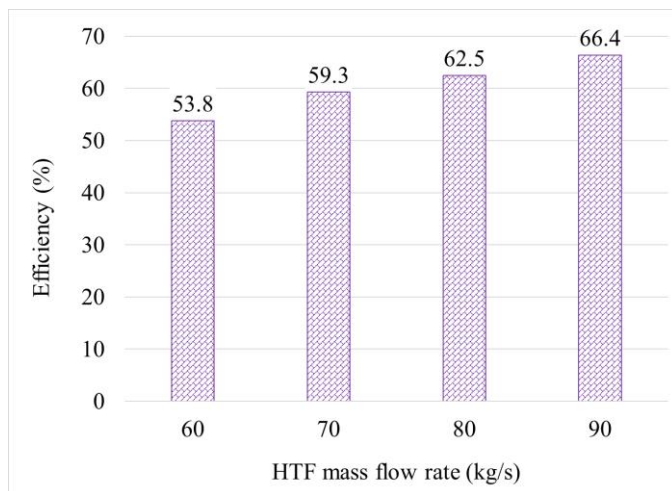


Figure 9. The effect of HTF flow rate on the thermal efficiency of the PDC enhanced with the PCM layers

5. CONCLUSIONS

In the present study, a novel solar receiver design with multiple layers of thin PCM was examined. The PCM layers were inserted between the passages of the working fluid. The solar flux distribution on the receiver was determined based on the discrete ordinate radiation model. The coupled governing equations including mass, momentum, energy, and phase change were solved numerically within a 3D domain.

According to the results, by increasing the HTF flow rate from 60 to 90 kg/h, the system efficiency was increased from 53.8 to 66.4 %.

The temperature increase rate did not remain unchanged along the passage of the flow stream.

In the outer loop, the temperature had an average increase rate of 2.8 °C. However, in the middle flow loop, the temperature increased to about 8.8 °C and the temperature growth in the central section was 9.5 °C.

Moreover, the presence of multilayer PCM fields managed to preserve the uniform pattern of thermal energy absorption even in the intermittent or full cloudy sky.

An experimental setup should be established to measure the experimental data and to compare them with the results of numerical simulation.

6. ACKNOWLEDGEMENT

The paper has not received any external funding and thus, there is nothing to be acknowledged.

NOMENCLATURE

\vec{v}_{pull}	Pull velocity (m/s)
h_s	Sensible enthalpy (J/kg)

h_t	Total enthalpy (J/kg)
A_{mz}	Mushy zone coefficient
\vec{S}	Source term in the momentum equation ($kg/m^2 \cdot s^2$)
T_0	Reference temperature (k)
\vec{v}	Velocity vector (m/s)
c_p	Specific heat ($J/kg \cdot k$)
\vec{g}	Gravitational acceleration (m/s^2)
\dot{q}	Volumetric heat generation rate (W/m^3)
P	Pressure (pa)
T	Temperature (k)
k	Conductivity ($W/m \cdot k$)
t	Time (s)

Greek letters

α	Liquid fraction
β	Coefficient of volume expansion (k^{-1})
ε	Non-zero small number
μ	Viscosity ($kg/m \cdot s$)
ρ	Density (kg/m^3)

REFERENCES

1. Avargani, V.M., Rahimi, A. & Tavakoli, T. (2016). Exergetic optimization and optimum operation of a solar dish collector with a cylindrical receiver. *Journal of Energy Engineering*, Vol 142, 04015049. [https://doi.org/10.1061/\(ASCE\)EY.1943-7897.0000322](https://doi.org/10.1061/(ASCE)EY.1943-7897.0000322).
2. Felemban, B. F., Essa, F. A., Afzal, A. Ahmed, M. H., Saleh, B., Panchal, H., Shanmugan, S., Ammar Elsheikh, A. & Omara, Z. M. (2022). Experimental investigation on dish solar distiller with modified absorber and phase change material under various operating conditions. *Environmental Science and Pollution Research*, Vol. 29, 63248–63259. <https://doi.org/10.1007/s11356-022-20285-z>.
3. Kabeel, A. E., Elkelawy, M., Mohamad, H. A., Elbanna, A. M., Panchal, H., Suresh, M. & Israr, M. (2022). The influences of loading ratios and conveying velocity on gas-solid two phase flow characteristics: a comprehensive experimental CFD-DEM study. *International Journal of Ambient Energy*, Vol. 43, 2714-2726. <https://doi.org/10.1080/01430750.2020.1758777>.
4. Khalil Anwar, M., Yilbas, B.S. & Shuja, S.Z. (2016). A thermal battery mimicking a concentrated volumetric solar receiver. *Applied Energy*, Vol. 125, 17516–30. <https://doi.org/10.1016/j.apenergy.2016.04.110>.
5. Kopalakrishnaswami, A.S. & Natarajan, S.K. (2022). Comparative study of modified conical cavity receiver with other receivers for solar paraboloidal dish collector system. *Environmental Science and Pollution Research*, Vol. 29, 7548-7558. <https://doi.org/10.1007/s11356-021-16127-z>.
6. Kousik, S. S. & Natarajan, S. K. (2022). Combined enhancement of evaporation and condensation rates in the solar still for augmenting the freshwater productivity using energy storage and natural fibres. *AQUA - Water Infrastructure, Ecosystems and Society*, Vol. 71, 628–641. <https://doi.org/10.2166/aqua.2022.017>.
7. Mawire, A., Lentswe, K.A. & Shobo, A. (2019). Performance comparison of four spherically encapsulated phase change materials for medium temperature domestic applications. *Journal of Energy Storage*, Vol. 23, 469–479. <https://doi.org/10.1016/j.est.2019.04.007>.
8. Mazzucco, G., Xott, G., Salomoni, V.A., Majorana, C.E., Giannuzzi, G.M. & Miliozzi, A. (2018). Modeling techniques of storage modules with PCM microcapsules: case study. *Journal of Energy Engineering*, Vol. 144, 05017005. [https://doi.org/10.1061/\(ASCE\)EY.1943-7897.0000501](https://doi.org/10.1061/(ASCE)EY.1943-7897.0000501).

9. Natarajan, S., Raviteja, B., Sri Harshavardhan, D., Hari Prasath, G. & Suraparaju, S. K. (2019). Numerical study of natural convection in flat receiver with and without secondary reflector for solar parabolic dish system. *IOP Conference Series: Earth and Environmental Science*, Volume 312, National Conference on Recent Advances in Fuel Cells and Solar Energy 11–12 May 2019, Karaikal, U.T of Puducherry, India, 012020. <https://doi.org/10.1088/1755-1315/312/1/012020>.
10. Reddy, K.& Kumar, N.S. (2009). Convection and surface radiation heat losses from modified cavity receiver of solar parabolic dish collector with two-stage concentration. *Heat Mass Transfer*, Vol. 45, 363–373. <https://doi.org/10.1007/s00231-008-0440-2>.
11. Palanikumar, G., Sengottain, S., Chithambaram, V., Gorjian, S., Pruncu, C., Essa, F., Kabeel, A. E., Panchal, H., Balasundaram, J., Ebadi, H., Elsheikh, A.& Selvaraju, P. (2021). Thermal Investigation of a Solar Box-type Cooker with Nanocomposite Phase Change Materials Using Flexible Thermography. *Renewable Energy*, Vol. 178, 260-282. <https://doi.org/10.1016/j.renene.2021.06.022>.
12. Panchal, H. N. & Patel, N. (2018). ANSYS CFD and experimental comparison of various parameters of a solar still. *International Journal of Ambient Energy*, Vol. 39, 551-557. <https://doi.org/10.1080/01430750.2017.1318785>.
13. Panchal, H., Patel, K., Elkelay, M. & Bastawissi, H. A. (2021). A use of various phase change materials on the performance of solar still: a review. *International Journal of Ambient Energy*, Vol. 42, 1575-1580. <https://doi.org/10.1080/01430750.2019.1594376>.
14. Peiro, G., Gasia, J., Mir, L. & Cabeza, L.F. (2018). Experimental evaluation at pilot plant scale of multiple PCM (cascaded) vs. single PCM configuration for thermal energy storage. *Renewable Energy*, Vol. 83, 729–736. <https://doi.org/10.1016/j.renene.2015.05.029>.
15. Ren, Y., Qi, H., Shi, J., Chen, Q., Wang, Y. & Ruan, L. (2018). Thermal performance characteristics of porous media receiver exposed to concentrated solar radiation. *Journal of Energy Engineering*, Vol. 143, 04017013. [https://doi.org/10.1061/\(ASCE\)EY.1943-7897.0000448](https://doi.org/10.1061/(ASCE)EY.1943-7897.0000448).
16. Saleh, B., Essa, F. A., Aly, A., Aleshli, M., Panchal, H., Afzal, A. & Shanmugan, S. (2022). Investigating the performance of dish solar distiller with phase change material mixed with Al₂O₃ nanoparticles under different water depths. *Environmental Science and Pollution Research*, Vol. 29, 28115–28126. <https://doi.org/10.1007/s11356-021-18295-4>.
17. Saleem, U., Aziz, M.S., Waqas, A. & Hanif, M.A. (2018). Heat energy transfer using butyl stearate as phase change material for free-cooling applications. *Journal of Energy Engineering*, Vol. 144, 04018043. <https://doi.org/10.1061/%28ASCE%29EY.1943-7897.0000562>.
18. Sampathkumar, A.& Natarajan, S.K (2022). Experimental analysis on single slope solar still by the inclusion of Agar-Agar (Eucheuma) Fibre and micro Phase Change Material for the productivity enhancement. *Journal of Energy Storage*, Vol. 50, 104284. <https://doi.org/10.1016/j.est.2022.104284>.
19. Senthil, R. & Cheralathan, M. (2019). Enhancement of the thermal energy storage capacity of a parabolic dish concentrated solar receiver using phase change materials. *Journal of Energy Storage*, Vol. 25, 100841. <https://doi.org/10.1016/j.est.2019.100841>.
20. Santhi Rekha, S.M. & Sukchai, S. (2018). Design of phase change material based domestic solar cooking system for both indoor and outdoor cooking applications. *Journal of Solar Energy Engineering*, Vol. 140, (2018), <https://doi.org/10.1115/1.4039605>.
21. Singh, A.K & Natarajan, S.K. (2021). Thermal analysis of modified conical cavity receiver for a paraboloidal dish collector system. *Energy Sources, Part A: Recovery, Utilization, and Environmental Effects*, Vol. 1, 121,134. <https://doi.org/10.1080/15567036.2021.2017516>.
22. Sonawane, C., Alrubaie, A. J., Panchal, H., Chamkha, A. J., Jaber, M. M., Oza, A. D., Zahmatkesh, S., Burduhos-Nergis, D. D. & Burduhos-Nergis, D. P. (2022). Investigation on the Impact of Different Absorber Materials in Solar Still Using CFD Simulation—Economic and Environmental Analysis. *Water*, Vol. 14, 3031. <https://doi.org/10.3390/w14193031>.
23. Sonawane, C. R., Panchal, H. N., Hoseinzadeh, S., Ghasemi, M. H., Alrubaie, A. J. and Sohani, A. (2022). Bibliometric Analysis of Solar Desalination Systems Powered by Solar Energy and CFD Modelled. *Energies*, Vol. 15, 5279. <https://doi.org/10.3390/en15145279>.
24. Suraparaju, S.K, Sampathkumar, A & Natarajan, S.K. (2021). Experimental and economic analysis of energy storage-based single-slope solar still with hollow-finned absorber basin. *Heat Transfer*, Vol. 50, 5516– 5537. <https://doi.org/10.1002/htj.22136>.
25. Suraparaju, S.K.& Natarajan, S.K. (2021). Experimental investigation of single-basin solar still using solid staggered fins inserted in paraffin wax PCM bed for enhancing productivity. *Environmental Science and Pollution Research*, Vol. 28, 20330–20343. <https://doi.org/10.1007/s11356-02>.
26. Suraparaju, S.K. &Natarajan, S.K. (2021). Productivity enhancement of single-slope solar still with novel bottom finned absorber basin inserted in phase change material (PCM): techno-economic and enviro-economic analysis. *Environmental Science and Pollution Research*, Vol. 28, 45985–46006. <https://doi.org/10.1007/s11356-021-13495-4>.
27. Taumoefolau, T., Paitoonsurikarn, S., Hughes, G. & Lovegrove, K., (2021). Experimental investigation of natural convection heat loss from a model solar concentrator cavity receiver. *Journal of Solar Energy Engineering*, Vol. 126, 801–807. <https://doi.org/10.1115/1.1687403>.
28. Thakur, A. K., Singh, R., Gehlot, A., Kaviti, A. K., Aseer, R., Suraparaju, S. K., Natarajan, S. K., & Sikarwar, V. S. (2022). Advancements in solar technologies for sustainable development of agricultural sector in India: a comprehensive review on challenges and opportunities", *Environmental Science and Pollution Research*, Vol. 29, 43607–43634. <https://doi.org/10.1007/s11356-022-20133-0>.
29. Tharun, M., Navin, S.R., Arjun Singh, K., Sampathkumar, A. & Natarajan, S.K. (2022). Numerical Comparison of Elliptical and Conical Cavity Receiver of Solar Parabolic Dish Collector System. In: Govindan, K., Kumar, H., Yadav, S. (eds). *Advances in Mechanical and Materials Technology*, International Conference on Energy, Materials Sciences & Mechanical Engineering EMSME 2020: Advances in Mechanical and Materials Technology pp 607–618. https://doi.org/10.1007/978-981-16-2794-1_53.
30. Varun, K., Arunachala, U.C. & Elton, D.N. (2020). Trade-off between wire matrix and twisted tape: SOLTRACE® based indoor study of parabolic trough collector. *Renewable Energy, Elsevier*, Vol. 156, 478-492. <https://doi.org/10.1016/j.renene.2020.04.093>.
31. Yilbasa, B.S. and Khalil Anwar, M. (2016). Design of a mobile thermal battery and analysis of thermal characteristics. *Journal of Renewable and Sustainable Energy*, Vol. 8, 024102. <https://doi.org/10.1063/1.4943662>.